Regenerative Therapy 14 (2020) 299–305

Contents lists available at ScienceDirect

Regenerative Therapy

journal homepage: http://www.elsevier.com/locate/reth

Original Article

Imaging of lysophosphatidylcholine in an induced pluripotent stem cell-derived endothelial cell network

Yasuo Shimizu [a, *], Yusuke Nakamura [a], Yasuhiro Horibata [b], Mio Fujimaki [a], Keitaro Hayashi [c], Nobuhiko Uchida [a], Hiroko Morita [a], Ryo Arai [a], Kazuyuki Chibana [a], Akihiro Takemasa [a], Hiroyuki Sugimoto [b]

[a] Department of Pulmonary Medicine and Clinical Immunology, Dokkyo Medical University School of Medicine, 880 Kitakobayashi, Mibu, Tochigi, 321-0293, Japan
[b] Department of Biochemistry, Dokkyo Medical University School of Medicine, 880 Kitakobayashi, Mibu, Tochigi, 321-0293, Japan
[c] Department of Pharmacology and Toxicology, Dokkyo Medical University School of Medicine, 880 Kitakobayashi, Mibu, Tochigi, 321-0293, Japan

ARTICLE INFO

Article history:
Received 11 January 2020
Received in revised form
1 March 2020
Accepted 11 March 2020

Keywords:
Endothelial
Imaging
Pluripotent
Lysophosphatidylcholine
MALDI
Stem

ABSTRACT

Introduction: Vascular endothelial cell disorders are closely related to cardiovascular disease (CVD) and pulmonary diseases. Abnormal lipid metabolism in the endothelium leads to changes in cell signalling, and the expression of genes related to immunity and inflammation. It is therefore important to investigate the pathophysiology of vascular endothelial disorders in terms of lipid metabolism, using a disease model of endothelium.

Methods: Human induced pluripotent stem cell-derived endothelial cells (iECs) were cultured on a matrigel to form an iEC network. Lipids in the iEC network were investigated by matrix-assisted laser desorption/ionization (MALDI) time-of-flight (TOF) imaging mass spectrometry (IMS) analysis. Ion fragments obtained by mass spectrometry were analysed using an infusion method, involving precursor ion scanning with fragment ion.

Results: The MALDI TOF IMS analysis revealed co-localized intensity of peaks at *m*/*z* 592.1 and 593.1 in the iEC network. Tandem mass spectrometry (MS/MS) analysis by MALDI-imaging, in conjunction with precursor ion scanning using an infusion method with lipid extracts, identified that these precursor ions were lysophosphatidylcholine (LPC) (22:5) and its isotype.

Conclusion: The MALDI-imaging analysis showed that LPC (22:5) was abundant in an iEC network. As an in vitro test model for disease and potential therapy, present analysis methods using MALDI-imaging combined with, for example, mesenchymal stem cells (MSC) to a disease derived iEC network may be useful in revealing the changes in the amount and distribution of lipids under various stimuli.

1. Introduction

Lipids are involved in various cellular functions and play a role in homeostasis and disease states [1–3]. Several lipid species in lipid classes such as fatty acids (FAs), phospholipids (PLs), and ceramides (CMs) have been proposed as useful biomarkers in early identification of disease [4,5]. Endothelial cells (ECs) are recognized as multifunctional cells involved in: regulating the transfer of oxygen; nutrients; coagulation; vascular tone; angiogenesis; stimulating smooth muscle cells and fibroblasts, and the vasculature composition of normal and/or tumor microenvironments [6–8]. External stresses, such as oxidative, glycative or lipoxidative, can alter lipid profiles in ECs compared to the homeostatic state [6,9]. Lipidomics has become a field of research as a result of technological advances in analytical tools of mass spectrometry (MS), nuclear magnetic resonance (NMR), high-performance of liquid chromatography (HPLC), and imaging mass spectrometry (IMS) [10,11]. These techniques identify unique lipid species that indicate potential adverse cardiovascular events. Specifically,

* Corresponding author. Department of Pulmonary Medicine and Clinical Immunology, Dokkyo Medical University School of Medicine, 880 Kitakobayashi, Mibu, Tochigi 321-0293, Japan.Fax: +81 282 86 5080
E-mail address: yasuo-s@dokkyomed.ac.jp (Y. Shimizu).

Peer review under responsibility of the Japanese Society for Regenerative Medicine.

https://doi.org/10.1016/j.reth.2020.03.007

phosphatidylcholine (PC) (32:0) and sphingomyelin (SM) (16:0) have been associated with mortality in cardiovascular disease (CVD) [12], and lysophosphatidylcholine (LPC) (18:1) and (18:2) has been shown to be associated with incidents of CVD [13]. The dysfunction of ECs can result in atherosclerosis [14] and IMS has revealed increased levels of LPC, phosphatidic acid (PA), PC and SM in aortic tissue [15,16].

Induced pluripotent stem cell (iPSC)-derived differentiated cells have been used for drug discovery, drug repositioning and toxicological screening of drugs [17]. Currently, iPSC-derived cell therapy is being used to investigate age-related macular degeneration (AMD), Parkinson's disease (PD), fibro dysplasia ossificans progressiva (FOP) and spinal cord injury (SCI) [18–21]. In rats, disease models of idiopathic or heritable pulmonary hypertension (IPAH/HPAH), X-linked adrenoleukodystrophy (X-ALD), lipopolysaccharide-induced acute lung injury using induced pluripotent stem cell-derived endothelial cells (iECs) have been reported [22–24]. The investigation of IPAH/HPAH in this model revealed a reduction in the expression of several genes that may play a role in the effectiveness of treatment by affecting drug repositioning [22].

The first report investigating lipid accumulation was conducted in a blood brain barrier (BBB) model consisting of human brain microvascular iECs derived from childhood cerebral-ALD (cc-ALD) ECs. This study showed increased lipid accumulation as evaluated by Oil-Red-O staining in the BBB [23]. The specific lipid classes or clinical meanings of an increase in lipids in iECs remains, however, unknown.

Lipids are closely related to clinical information in disease states, therefore disease models using iECs may be useful in investigating the role of lipids in disease states to provide patients with more effective therapeutic treatments.

In the present study, an iEC network culture model was generated from human normal iECs. The two-dimensional lipid distribution was examined in the iEC network by IMS. A co-culture model with lung tissue from human pulmonary mesenchymal stem cells (HPMSC) and the iEC network was also analyzed. The findings from this present study indicate that IMS analysis of lipids in a disease-derived iEC network model may be beneficial in identifying patients at risk of CVD and providing more effective treatment for these patients.

2. Materials and methods

2.1. Cell culture of iPSC-derived endothelial cell network on indium/tin oxide-coated (ITO) glass slides

Human iPSC derived endothelial cells (iECs) were obtained from Cellular Dynamics Inc (iCell®, Wisconsin, U.S.A). The iECs were cultured in medium of VascuLife® VEGF Comp Kit (Lifeline Cell Technology, CA, U.S.A) as previously [25]. For IMS analysis, iECs were cultured in Matrigel® (Corning, NY, U.S.A) on indium/tin oxide-coated (ITO) glass slides (Sigma–Aldrich, U.S.A) in Quadri-PERM® 4-Compartment Culture Dish (Greiner Bio One, Austria). Briefly, the culture dish was kept at 4 °C , and the ITO glass slide was placed in the culture dish. The matrigel was then placed onto the cold ITO glass, and extended thinly by swing on ice. The ITO glass slide was then incubated in CO_2 at 37 °C for 30 min. Following this, 80% confluent cultured iECs were washed three times with phosphate buffered saline (PBS) at room temperature (RT), then treated with 0.025% phenol free trypsin (NAKARAI, Japan) for 2–3 min, and harvested by cell scraper. The collected iECs were centrifuged at 1000 rpm for 5 min, and stored in 1.5×10^5/ml in culture medium at 37 °C. A total of 500 μl of 1.5×10^5/ml iECs were placed onto matrigel-mounted ITO glass slides, and incubated in CO_2 at 37 °C for 1 h. After 1 h incubation, 6 ml of 37 °C culture medium was added to the culture dish to cover the surface of cells on the ITO glass slide. After 48 h culture (CO_2 at 37 °C), the ITO glass slides were removed from the culture dish and washed three times by cold saline (Otsuka Pharmaceutical, Japan). The iEC network was identified by microscopic examination (BZ-X, KEYENCE, Japan) and the glass slide snap frozen at −80 °C with desiccant of silica until use. Control samples of matrigel on ITO glass slides were prepared in a similar manner, minus iECs. The HPMSCs were cultured in mesenchymal stem cell medium (MSCM) in accordance with the manufacturer's instructions (ScienCells Research laboratory, CA, U.S.A). For co-culture with the iEC network and HPMSC (ScienCells Research laboratory, CA, U.S.A), the iEC network formation was prepared prior to adding HPMSCs. The HPMSCs were labelled with CellLight™ –mitochondria GFP, BacMam 2.0 (Fischer Scinentific, U.S.A) for 45 min according to the manufacturer's instructions, and treated with 0.125% trypsin–EDTA (Invitrogen), and harvested. Following centrifugation at 1000 rpm for 5 min, HPMSCs were transferred into the iEC network on the ITO glass slide at the concentration of 1×10^4 with 50%/50% volume culture medium of VascuLife®/MSCM and incubated for 48 h. After 48 h of culture, the ITO glass slides were removed from the culture dish and washed three times with cold saline. The contact areas between the iEC network and green fluorescent protein (GFP)-HPMSCs were identified using a fluorescence microscope (BZ-X, KEYENCE).

2.2. MALDI TOF IMS

The MALDI TOF IMS analysis was performed with an iMScope-TRIO® (SHIMADZU, Japan) equipped with a 355 nm Nd:YAG laser, as previously described [26]. The ITO glass slide stored at −80 °C, was left at RT to air dry. The iEC network was traced on the screen monitor using a microscope equipped with iMScopeTRIO® (SHIMADZU, Japan). The inside of the traced area was then analyzed with MALDI-imaging analysis. The ITO glass slide was then homogenously coated with a matrix (2-hydroxy-5-methoxybenzoic acid: DHB) using an iMLayer® (SHIMADZU, Japan). The MS data were acquired in positive ion mode in the mass range m/z 500 to 1000. A laser beam diameter was set at 5 μm, and mass resolving power was 10,000 at m/z 1000 used in MS and tandem MS/MS scans. Principal component analysis (PCA) and hierarchical clustering analysis (HCA) of image patterns was performed as previously described [26]. The target m/z was determined after comparison with the m/z peaks derived from the control matrigel without iECs. A sample ITO glass slide without iECs but coated with matrigel was prepared in a similar manner and used as a control.

2.3. Extraction of lipids in ECs network for LC-MS and database research

The ITO glass slide was washed three times in cold saline, and the matrigel, including the iEC network, was treated with cell recovery solution according to the manufacturer's instructions (Corning NY, U.S.A.). The iECs were then collected. After sonication of the cells, lipids were extracted by the Bligh-Dyer method as previously described [26]. Samples were stored at −80 °C after sealing under nitrogen. To identify the unknown lipids co-localized in the iEC network, lipid extracts were subjected to the infusion method, using a high sensitivity precursor scanning with fragment ion [27], referencing fragment ions from tandem MS/MS analysis by MALDI-imaging. The LipidView™ database with QTRAP5500 mass spectrometer (Sciex Inc., Framingham, MA USA) was used to determine specific ions.

2.4. Statistical analysis

The PCA was performed for the cumulative contribution ratio of PC > 80% in each image and the contribution of PC value in each group >mean PC value of each image. The HCA was performed in accordance with the Euclidean distance and the Ward Method. The PCA, HCA, and generation of dendrograms were performed using iMScopeTRIO® (SHIMADZU, Japan) software.

3. Results

3.1. MALDI-imaging analysis of iEC network

Formation of the iEC network or matrigel without iEC on an ITO glass slide was confirmed by microscopic examination before being stored at −80 °C (Fig. 1a–c). The ITO glass slides were air dried, and the iEC network traced using microscopy equipped with iMScopeTRIO® (SHIMADZU, Japan). The inside of the traced area was analyzed in regards to the iEC network (Fig. 1e) or in the matrigel without the iEC network (Fig. 1f). The MS analysis of the iEC network showed various intensities in *m/z* peaks including those derived from the matrigel and from the iEC network (Fig. 2a). High intensity of the peaks at *m/z* 545.0 and 585.0 were determined from DHB (Fig. 2b). The PCA analysis based on two−dimensional image patterns identified 24 groups (Supplemental data 1). PCA3 including peaks at *m/z* 592.1, 593.1, 632.3 and 728.1 were co-localized to the iEC network (Fig. 3a). The HCA analysis showed 13 clusters (Supplemental data 2). The following HCA measurements were co-localized with the iEC network: HCA10 of *m/z* 728.1; HCA11 of *m/z* 592.1 and 593.1; HCA12 of *m/z* 632.3, and HCA13 of *m/z* 672.4. Among the distribution of *m/z* 592.1, some spots were high in the iEC network as shown yellow to red dots (Fig. 3b). Furthermore, dendrogram of the HCA clusters demonstrated that these *m/z* peaks formed close trees (Fig. 4). These peaks of *m/z* were not observed on matrigel without the iEC network.

3.2. Tandem MS/MS analysis of peaks of m/z co-localized to iEC network

To confirm the lipids co-localized with the iEC network, tandem MS/MS analysis was performed on peaks of *m/z* 592.1, 593.1, 632.3, 672.4 and 728.1 b y MALDI-imaging analysis. From the tandem MS/MS analysis on *m/z* peaks of 592.1 and 593.1 as precursor, a peak at *m/z* 184.1, a specific fragment of phosphoryl choline ion, was obtained (Fig. 5a and b). From other precursor *m/z* peaks at 632.3, 672.4 and 728.1, valuable fragments *m/z* could not be obtained (Supplemental data 3). To identify target lipids of *m/z* peaks at 592.1 and 593.1, lipid extract from the iEC network underwent analysis using the infusion method. Phosphoryl choline *m/z* 184 -containing phospholipids were determined via a database search of Lipid-View™ equipped in QTRAP5500. Peaks at *m/z* 592.1 and 593.1 were identified as LPC 22:5 (569.34) + Na (23) and the isotype. Other peaks at *m/z* 632.3, 672.4, and 728.1 could not be identified in the database. Tandem MS/MS analysis for the peak of ion precursor at *m/z* 728.1 showed a fragment at *m/z* 669.4, with the difference between 728.1 and 669.4 being 58.7. The neutral loss (NL) of 58.7 Da could be NL of 59 Da, and NL of 59 Da is a well known fragment from the phosphatidylcholine (PC) species of trimethylamine [N(CH3)3]. Therefore, *m/z* 728.14 might be PCs, however, no lipids matched the database.

3.3. Co-culture model of the iEC network and HPMSC

After forming the iEC network, GFP-HPMSCs were added with culture medium. The GFP-HPMSCs were observed in the iEC network line or joint. A representative pattern of GFP-HPMSCs in the iEC network is shown (Supplemental data 4). MALDI-imaging analysis were done on co-culture model. Intensity of the peaks of *m/z* 592 and 672 co-localized to iEC network were identified but it was difficult to distinguish the metabolic differences between GFP-HPMSC and iEC, or a GFP-HPMSC effect on iEC network (Supplemental data 5 and 6).

4. Discussion

The MALDI-imaging analysis of the iEC network demonstrated differences in the relative intensity reflecting various peaks of *m/z*. Tandem MS/MS analysis by MALDI-imaging of the iEC network and infusion method analysis using lipid extract identified LPC (22:5), and it was abundant in iEC network. A proposed model of co-culture with an iEC network and HPMSCs was also demonstrated.

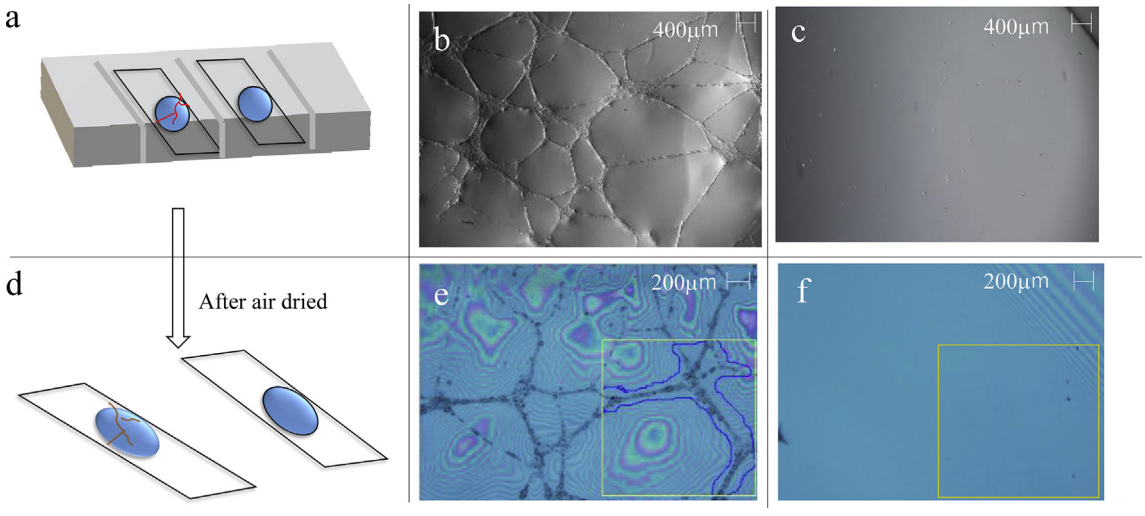

Fig. 1. Cell culture and preparation of slides for MALDI-imaging. Matrigel was mounted onto a sterilized ITO-coated glass slide and placed in a 4-compartment culture dish. Human iPSC-derived vascular endothelial cells (iECs) were cultured in matrigel for 2 days to form an iEC network (a). An ITO glass slide mounted with matrigel but without iECs underwent similar cell culture conditions (a). Microscopic analysis was performed on the iEC network (b) and the matrigel without the iEC network (c). The glass slide was washed 3 times with physiological saline, then stored at −80 °C with desiccant. On the day of MALDI-imaging analysis, the slide was air dried at RT (d). The iEC network (e) or the matrigel without the iEC (f) were again confirmed by microscope equipped with iMScopeTRIO® (SHIMADZU, Japan), and the area to irradiation determined by tracing technology. Inside of the blue line were irradiated in the iEC network (e), and inside of the yellow square were irradiated in matrigel without iEC (f). Scale bars in each panel indicate ranges from 200 to 400 μm.

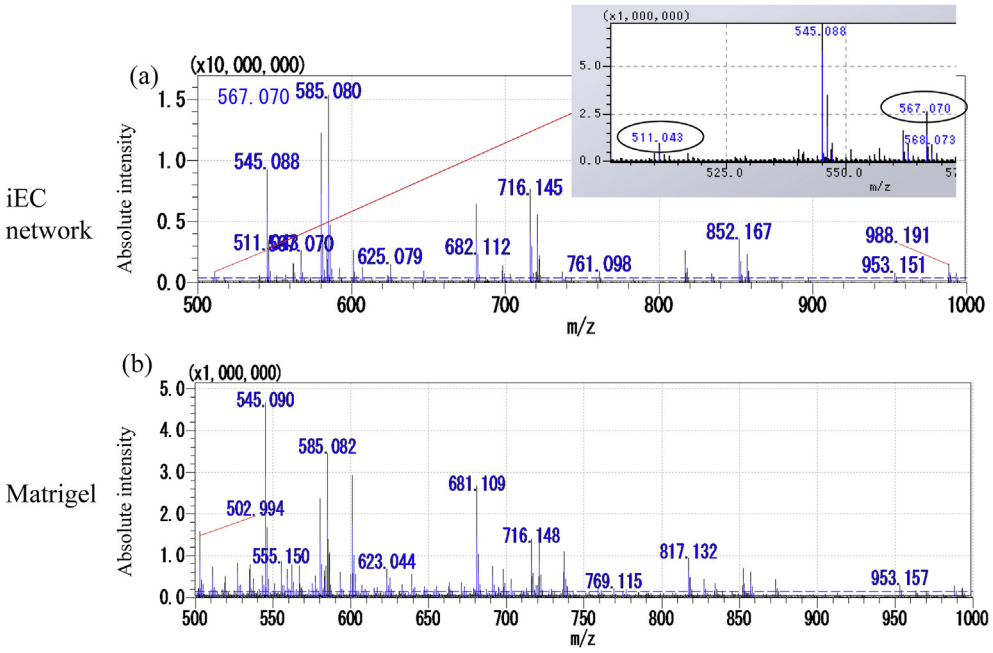

Fig. 2. MS analysis of the iEC network and matrigel. The high peaks of *m*/*z* 545.0, 585.0 were from the matrix of DHB in both samples of the iEC network (a) and the matrigel (b).

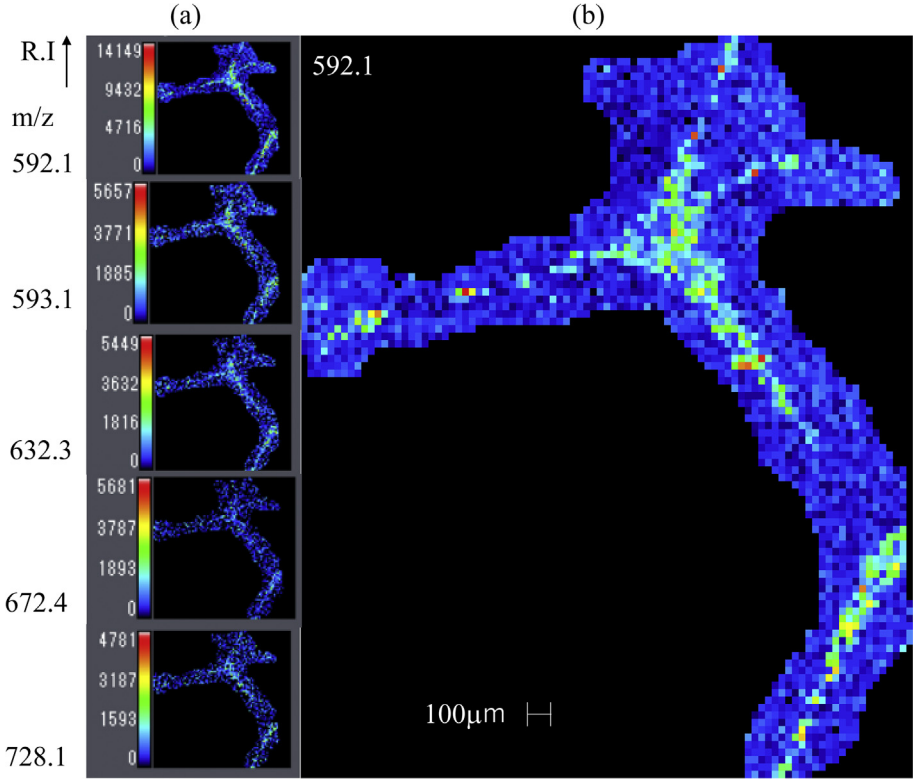

Fig. 3. PCA for the iEC network. PCA analysis indicated the 5 components in the iEC network (a). A peak of *m*/*z* 592.1 was detected in the iEC network, and various intensities of this were also observed (b).

One of the lysophospholipids generated from glycerophospholipid metabolism cleaved by phospholipase A2 or A1 is LPC is [28,29]. It is well known that LPC plays an important role in cell signaling, migration, proliferation and the release of cytokines in various types of cells including: ECs; adipocytes; hepatocytes; immune cells, and neuronal cells [30]. It has been shown that ECs can be activated by the following: LPC; induced monocyte chemoattractant protein-1 (MCP-1); interleukin-8 (IL-8); regulated on activation, normal T cell expressed and secreted (RANTES) expression, cytotoxicity or apoptosis, and oxidative stress [31–33].

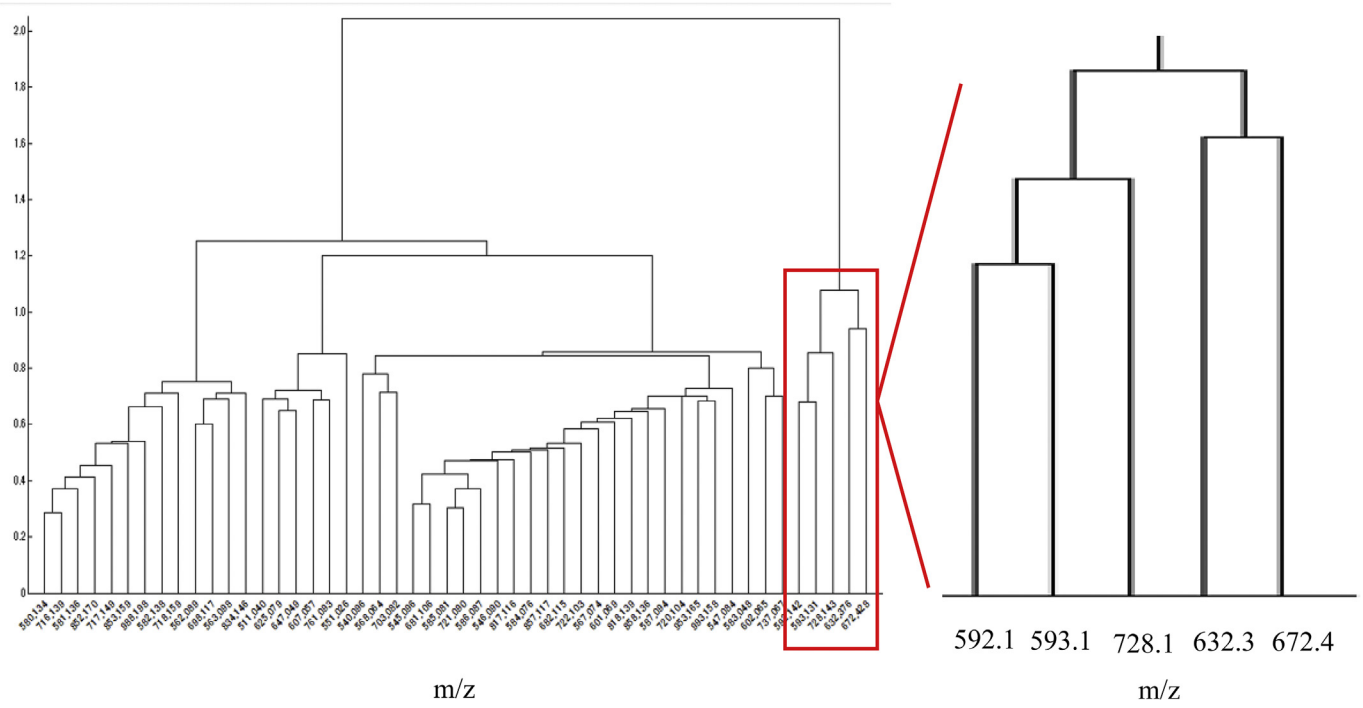

Fig. 4. Dendrogram of HCA cluster. HCA indicated *m/z* peaks in the iEC network (red square). These *m/z* peaks corresponded with the results of the PCA analysis.

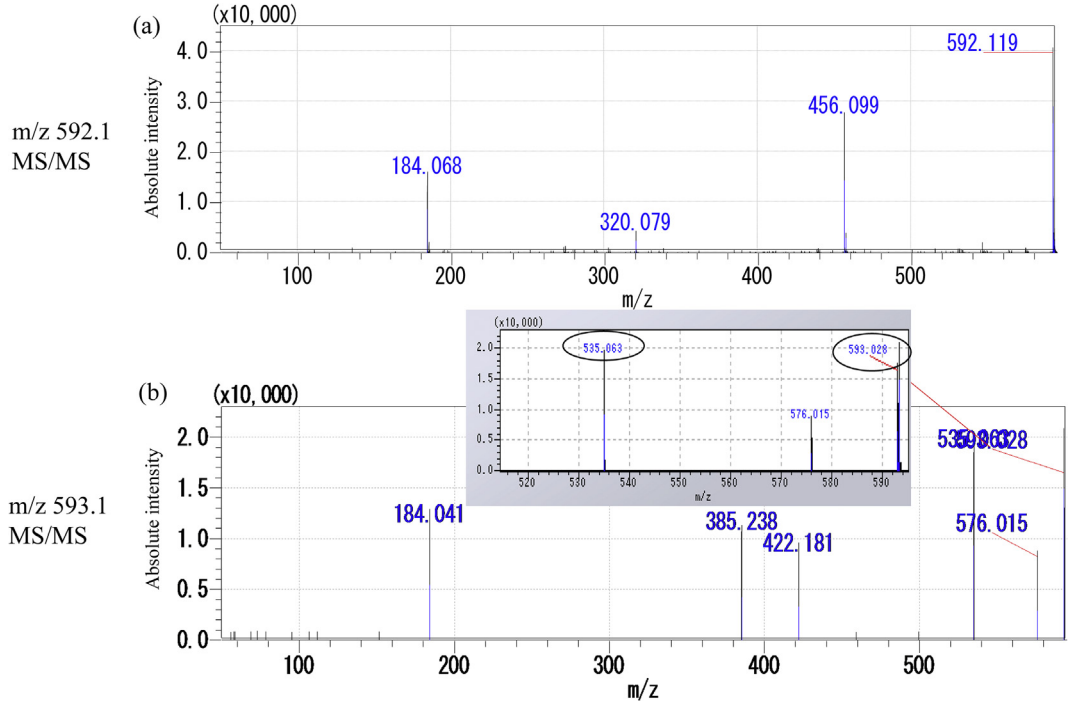

Fig. 5. Tandem MS/MS analysis for peaks of *m/z* 592.1 and 593.1. Both *m/z* peaks of 592.1 (a) and 593.1 (b) showed the head group of phosphoryl choline, *m/z* 184.0.

Interestingly, LPC has a potent property that can result in trans differentiation of human aortic ECs into innate immune cells via up-regulation of cytosolic calcium and mitochondrial reactive oxygen species (ROS) [34]. Furthermore, it has been reported that LPC may play a role in the induction of histone acetylation levels at H3K14 in 19 trained immunity genes in ECs. The acetylation status of H3K14 is currently considered a biomarker or therapeutic target of CVD, further supporting the need to consider LPC as a biomarker for CVD [35].

As a biomarker, LPC has been observed in the plasma, serum and other fluids in the following diseases: bronchoalveolar lavage fluid (BALF); lipid extraction of tissue in cystic fibrosis; idiopathic pulmonary fibrosis (IPF); chronic obstructive pulmonary disease (COPD) CVD; hepatic cancer; lung cancer patients, and asthma

[36–42]. In a murine bleomycin-induced pulmonary fibrosis model, LPC was reported to be associated the pathophysiology of this disease [30,43]. In the present study, LPC (22:5) was identified in an iEC network. Several LPCs, including LPC (14:0), (16.0), (18:0), (18:2), (20:4), (22:3) and (22:6) have been reported [30], however, few reports have identified LPC (22:5) [29,40,44]. In patients with hepatocellular carcinoma (HCC) LPC (22:5) levels were decreased which may indicate poorly differentiated HCC [40]. In a murine lung fibrosis experimental model, an increase in LPC (22:5) was observed in the lung, however, there was no increase in systemic LPC [29]. In addition, LPC (22:5) was produced from phospholipase A activity of PCs, and also by autotaxin (ATX) dependently, which was also elevated in the lung in the murine lung fibrosis experimental model [29]. The relationship between ECs and LPC is complex. The stimulation by the combination of LPC and ATX treatment has been shown to increase the permeability of human umbilical vein EC (HUVEC), and immunohistochemistry (IHC) has revealed that the area of vascular leakage was co-localized with ATX protein expression in a murine model of renal fibrosis [44]. The findings from the present study show that LPC (22:5) was abundant in ECs, and that injury to ECs may cause increased levels of LPC at the site of injury. This increase in LPC levels may exacerbate the vascular metabolic state.

The MALDI-imaging analysis can obtain two-dimensional data. Studies have been conducted investigating LPC distribution in injured ischemic rat brain, ischemic porcine kidney and restenosis in injured rat carotid artery [45–47]. These studies reported an increase in LPC (18:1) at the injured site, and that the LPC levels were increased compared to the control by the time course (day 0 to day 14 of injury) [47]. In addition, LPC (20:4) and (22:6) have also been identified in murine normal airway by nanospray desorption electrospray ionization MS coupled to shear force microscopy [48], however, there have been no reports of LPC (22:5) by MS imaging. The present study focused on the expression of LPC in an iEC network, composed of an iEC network developed on matrigel by cell culture. The difference between the present study and previous reports are that previous studies focused on tissue sections including various cells, and on larger cell areas other than the iEC network, and different matrix or ion-modes were used for analysis of LPC expression.

The present study reports findings of LPC expression using a co-culture cell model with HPMSCs and an iEC network. Several studies have reported metabolic changes of stem cell transplant by IMS analysis [49,50]. IMS analysis has revealed that glioma stem cell transplants to the murine brain lowers PA, diacylglycerol (DAG) metabolism [49], and bone marrow derived mesenchymal stem cells (BM-MSC) in injured left soleus muscle of rat altered protein changes at the transplant site [50]. Limitations of this study are lack of some comparison data in iEC network regarding oxidative, glycative or lipoxidative stresses with or without HPMSC. To efficacy of HPMSC on iEC network, those various stimulations and the observational experiments with time-course during co-culture would be needed. Taken together, the co-culture model reported in the current study may be useful in the evaluation of the HPMSC effects on the metabolic changes of disease derived iEC network, by stimulating various compound or using disease-derived iEC network, however, further experiments are needed for practical use.

5. Conclusion

The findings of the present study indicate that a model of co-culture iEC network and HPMSC may be beneficial in determining the expression of lipids in a disease state. Furthermore, LPC (22:5) was abundant in the iEC network, and MALDI-imaging analysis was useful in identifying the distribution of lipids in the iEC network.

Declaration of competing interest

None of the authors have any conflict of interests.

Acknowledgements

This work was partly supported by a grant-in-aid for the JSPS KAKENHI Grant to Y.S, Japan (16K09553).

Appendix A. Supplementary data

Supplementary data to this article can be found online at https://doi.org/10.1016/j.reth.2020.03.007.

References

[1] Spiegel S, Ntambi J. Editorial for BBRC lipidomics special issue. Biochem Biophys Res Commun 2018;504:iii.
[2] Nakamura Y, Shimizu Y. Induced pluripotent stem cells for regenerative medicine: quality control based on evaluation of lipid composition. Adv Exp Med Biol 2020;1212:49–56. https://doi.org/10.1007/5584_2019_394.
[3] Johnson AA, Stolzing A. The role of lipid metabolism in aging, lifespan regulation, and age-related disease. Aging Cell 2019;18:1–26. e13048. [Review].
[4] Kohno S, Keenan AL, Ntambi JM, Miyazaki M. Lipidomic insight into cardiovascular diseases. Biochem Biophys Res Commun 2018;504:590–5.
[5] Matanes F, Twal WO, Hammad SM. Sphingolipids as biomarkers of disease. Adv Exp Med Biol 2019;1159:109–38 [Review].
[6] Bierhansl L, Conradi LC, Treps L, Dewerchin M, Carmeliet P. Central role of metabolism in endothelial cell function and vascular disease. Physiology 2017;32:126–40.
[7] Datta M, Coussens LM, Nishikawa H, Hodi FS, Jain RK. Reprogramming the tumor microenvironment to improve immunotherapy: emerging strategies and combination therapies. Am Soc Clin Oncol Educ Book 2019;39:165–74 [Review].
[8] Martin JD, Seano G, Jain RK. Normalizing function of tumor vessels: progress, opportunities, and challenges. Annu Rev Physiol 2019;81:505–34.
[9] Colombo S, Melo T, Martínez-López M, Carrasco MJ, Domingues MR, Pérez-Sala D, et al. Phospholipidome of endothelial cells shows a different adaptation response upon oxidative, glycative and lipoxidative stress. Sci Rep 2018;8:12365.
[10] Lee HC, Yokomizo T. Applications of mass spectrometry-based targeted and non-targeted lipidomics. Biochem Biophys Res Commun 2018;504:576–81.
[11] Nampei M, Horikawa M, Ishizu K, Yamazaki F, Yamada H, Kahyo T, et al. Unsupervised machine learning using an imaging mass spectrometry dataset automatically reassembles grey and white matter. Sci Rep 2019;9:13213.
[12] Sigruener A, Kleber ME, Heimerl S, Liebisch G, Schmitz G, Maerz W. Glycerophospholipid and sphingolipid species and mortality: the Ludwigshafen risk and cardiovascular health (LURIC) study. PloS One 2014;9:1–8. e85724.
[13] Ganna A, Salihovic S, Sundstrom J, Broeckling CD, Hedman AK, Magnusson PK, et al. Large-scale metabolomic profiling identifies novel biomarkers for incident coronary heart disease. PLoS Genet 2014;10:e1004801.
[14] Gimbrone Jr MA, García-Cardeña G. Endothelial cell dysfunction and the pathobiology of atherosclerosis. Circ Res 2016;118:620–36.
[15] Martin-Lorenzo M, Balluff B, Maroto AS, Carreira RJ, van Zeijl RJ, Gonzalez-Calero L, et al. Lipid and protein maps defining arterial layers in atherosclerotic aorta. Data Brief 2015;4:328–31.
[16] Meisenbichler C, Doppler C, Bernhard D, Müller T. Improved matrix coating for positive- and negative-ion-mode MALDI-TOF imaging of lipids in blood vessel tissues. Anal Bioanal Chem 2019;411:3221–7.
[17] Karagiannis P, Takahashi K, Saito M, Yoshida Y, Okita K, Watanabe A, et al. Induced pluripotent stem cells and their use in human models of disease and development. Physiol Rev 2019;99:79–114 [Review].
[18] Mandai M, Kurimoto Y, Takahashi M. Autologous induced stem-cell-derived retinal cells for macular degeneration. N Engl J Med 2017;377:792–3.
[19] Kikuchi T, Morizane A, Doi D, Magotani H, Onoe H, Hayashi T, et al. Human iPS cell-derived dopaminergic neurons function in a primate Parkinson's disease model. Nature 2017;548:592–6.
[20] Nakajima T, Ikeya M. Insights into the biology of fibrodysplasia ossificans progressiva using patient-derived induced pluripotent stem cells. Regen Ther 2019;11:25–30 [Review].
[21] Nagoshi N, Tsuji O, Nakamura M, Okano H. Cell therapy for spinal cord injury using induced pluripotent stem cells. Regen Ther 2019;11:75–80 [Review].
[22] Sa S, Gu M, Chappell J, Shao NY, Ameen M, Elliott KA, et al. Induced pluripotent stem cell model of pulmonary arterial hypertension reveals novel gene expression and patient specificity. Am J Respir Crit Care Med 2017;195:930–41.
[23] Lee CAA, Seo HS, Armien AG, Bates FS, Tolar J, Azarin SM. Modeling and rescue of defective blood-brain barrier function of induced brain microvascular endothelial cells from childhood cerebral adrenoleukodystrophy patients. Fluids Barriers CNS 2018;15:9.

[24] Xing D, Wells JM, Giordano SS, Feng W, Gaggar A, Yan J, et al. Induced pluripotent stem cell-derived endothelial cells attenuate lipopolysaccharide-induced acute lung injury. J Appl Physiol 2019;127:444–56.
[25] Nakamura Y, Shimizu Y, Horibata Y, Tei R, Koike R, Masawa M, et al. Changes of plasmalogen phospholipid levels during differentiation of induced pluripotent stem cells 409B2 to endothelial phenotype cells. Sci Rep 2017;7:9377.
[26] Shimizu Y, Satou M, Hayashi K, Nakamura Y, Fujimaki M, Horibata Y, et al. Matrix-assisted laser desorption/ionization imaging mass spectrometry reveals changes of phospholipid distribution in induced pluripotent stem cell colony differentiation. Anal Bioanal Chem 2017;409:1007–16.
[27] Houjou T, Yamatani K, Nakanishi H, Imagawa M, Shimizu T, Taguchi R. Rapid and selective identification of molecular species in phosphatidylcholine and sphingomyelin by conditional neutral loss scanning and MS3. Rapid Commun Mass Spectrom 2004;18:3123–30.
[28] Bou Khalil M, Hou W, Zhou H, Elisma F, Swayne LA, Blanchard AP, et al. Lipidomics era: accomplishments and challenges. Mass Spectrom Rev 2010;29:877–929.
[29] Black KE, Berdyshev E, Bain G, Castelino FV, Shea BS, Probst CK, et al. Autotaxin activity increases locally following lung injury, but is not required for pulmonary lysophosphatidic acid production or fibrosis. Faseb J 2016;30:2435–50.
[30] Law SH, Chan ML, Marathe GK, Parveen F, Chen CH, Ke LY. An updated review of lysophosphatidylcholine metabolism in human diseases. Int J Mol Sci 2019;20:1–24. pii: E1149 [Review].
[31] Takahara N, Kashiwagi A, Maegawa H, Shigeta Y. Phsophosphatidylcholine stimulates the expression and production of MCP-1 by human vascular endothelial cells. Metabolism 1996;45:559–64.
[32] G1 Murugesan, Sandhya Rani MR, Gerber CE, Mukhopadhyay C, Ransohoff RM, Chisolm GM, et al. Lysophosphatidylcholine regulates human microvascular endothelial cell expression of chemokines. J Mol Cell Cardiol 2003;35:1375–84.
[33] Chang MC, Lee JJ, Chen YJ, Lin SI, Lin LD, Jein-Wen Liou E, et al. Lysophosphatidylcholine induces cytotoxicity/apoptosis and IL-8 production of human endothelial cells: related mechanisms. Oncotarget 2017;8:106177–89.
[34] Li X, Wang L, Fang P, Sun Y, Jiang X, Wang H, et al. Lysophospholipids induce innate immune transdifferentiation of endothelial cells, resulting in prolonged endothelial activation. J Biol Chem 2018;293:11033–45.
[35] Lu Y, Sun Y, Drummer 4th C, Nanayakkara GK, Shao Y, Saaoud F, et al. Increased acetylation of H3K14 in the genomic regions that encode trained immunity enzymes in lysophosphatidylcholine-activated human aortic endothelial cells - novel qualification markers for chronic disease risk factors and conditional DAMPs. Redox Biol 2019;24:101221.
[36] Ollero M, Astarita G, Guerrera IC, Sermet-Gaudelus I, Trudel S, Piomelli D, et al. Plasma lipidomics reveals potential prognostic signatures within a cohort of cystic fibrosis patients. J Lipid Res 2011;52:1011–22.
[37] Rindlisbacher B, Schmid C, Geiser T, Bovet C, Funke-Chambour M. Serum metabolic profiling identified a distinct metabolic signature in patients with idiopathic pulmonary fibrosis - a potential biomarker role for LysoPC. Respir Res 2018;19:7.
[38] Deeb RS, Walters MS, Strulovici-Barel Y, Chen Q, Gross SS, Crystal RG. Smoking-associated disordering of the airway basal stem/progenitor cell metabotype. Am J Respir Cell Mol Biol 2016;54:231–40.
[39] Bandu R, Mok HJ, Kim KP. Phospholipids as cancer biomarkers: mass spectrometry-based analysis. Mass Spectrom Rev 2018;37:107–38.
[40] Zhang L, Huang Y, Lian M, Fan Z, Tian Y, Wang Y, et al. Metabolic profiling of hepatitis B virus-related hepatocellular carcinoma with diverse differentiation grades. Oncol Lett 2017;13:1204–10.
[41] Tan Y, Yin P, Tang L, Xing W, Huang Q, Cao D, et al. Metabolomics study of stepwise hepatocarcinogenesis from the model rats to patients: potential biomarkers effective for small hepatocellular carcinoma diagnosis. Mol Cell Proteomics 2012;11:M111. 010694.
[42] Kang YP, Lee WJ, Hong JY, Lee SB, Park JH, Kim D, et al. Novel approach for analysis of bronchoalveolar lavage fluid (BALF) using HPLC-QTOF-MS-based lipidomics: lipid levels in asthmatics and corticosteroid-treated asthmatic patients. J Proteome Res 2014;13:3919–29.
[43] Kulkarni YM, Dutta S, Iyer AKV, Wright CA, Ramesh V, Kaushik V, et al. A lipidomics approach to identifying key lipid species involved in vegf-inhibitor mediated attenuation of bleomycin-induced pulmonary fibrosis. Proteonomics Clin Appl 2018;12:e1700086.
[44] Sakai N, Bain G, Furuichi K, Iwata Y, Nakamura M, Hara A, et al. The involvement of autotaxin in renal interstitial fibrosis through regulation of fibroblast functions and induction of vascular leakage. Sci Rep 2019;9:7414.
[45] Koizumi S, Yamamoto S, Hayasaka T, Konishi Y, Yamaguchi-Okada M, Goto-Inoue N, et al. Imaging mass spectrometry revealed the production of lysophosphatidylcholine in the injured ischemic rat brain. Neuroscience 2010;168:219–25.
[46] van Smaalen TC, Ellis SR, Mascini NE, Siegel TP, Cillero-Pastor B, Hillen LM, et al. Rapid identification of ischemic injury in renal tissue by mass-spectrometry imaging. Anal Chem 2019;91:3575–81.
[47] Shi Y, Johnson J, Wang B, Chen B, Fisher GL, Urabe G, et al. Mass spectrometric imaging reveals temporal and spatial dynamics of bioactive lipids in arteries undergoing restenosis. J Proteome Res 2019;18:1669–78.
[48] Nguyen SN, Sontag RL, Carson JP, Corley RA, Ansong C, Laskin J. Towards high-resolution tissue imaging using nanospray desorption electrospray ionization mass spectrometry coupled to shear force microscopy. J Am Soc Mass Spectrom 2018;29:316–22.
[49] Wildburger NC, Wood PL1, Gumin J, Lichti CF2, Emmett MR2, Lang FF, et al. ESI-MS/MS and MALDI-IMS localization reveal alterations in phosphatidic acid, diacylglycerol, and DHA in glioma stem cell xenografts. J Proteome Res 2015;14:2511–9.
[50] Klein O, Strohschein K, Nebrich G, Fuchs M, Thiele H, Giavalisco P, et al. Unraveling local tissue changes within severely injured skeletal muscles in response to MSC-based intervention using MALDI Imaging mass spectrometry. Sci Rep 2018;8:12677.